

## INTERACTION OF HISTORICAL LEAD GLAZES WITH CORROSIVE MEDIA

MÁRIA KOLÁŘOVÁ\*, ALEXANDRA KLOUŽKOVÁ\*, KATEŘINA STODOLOVÁ\*,  
JAROSLAV KLOUŽEK\*\*, \*\*\*, PAVLA DVOŘÁKOVÁ\*, MARTINA KOHOUTKOVÁ\*\*\*\*

\*Department of Glass and Ceramics, University of Chemistry and Technology Prague, Technická 5, 166 28 Prague 6, Czech Republic

\*\*Laboratory of Inorganic Materials, University of Chemistry and Technology Prague, Technická 5, 166 28, Prague 6, Czech Republic

\*\*\*Institute of Rock Structure and Mechanics of the Czech Academy of Sciences, V Holešovičkách 41, 182 09, Prague 8, Czech Republic

\*\*\*\*Central Laboratories, University of Chemistry and Technology Prague, Technická 5, 166 28 Prague 6, Czech Republic

#E-mail: kavanovm@vscht.cz

Submitted August 20, 2021; accepted October 25, 2021

**Keywords:** Lead glazes, Corrosion mechanism, Microscopy, Spectroscopy, Historical ceramics

*Lead glasses and glazes are often discussed in terms of degradation processes in connection with their wide use in the field of cultural heritage in historical objects of low-fired glazed ceramics and historical glasses. This work is focused on the evaluation of the interaction of lead glazes with a corrosive media simulating environment of waste pits, deposits and possibly inappropriate conservation interventions. The first part of the experiment contains surface characterisation of several archaeological fragments of glazed ceramics. Two model lead silicate fritted glazes for corrosion tests were prepared based on their compositions. A system based on nitric acid solution simulates nitrates in the soil that surround the archaeological finds, and the aqueous solution of acetic acid represents corrosion in complex organic acids and humic acids. The concentration of Pb and Si was determined in corrosive solution by AAS. Precipitates were identified by optical microscopy (OM) and were examined via XRD and SEM-EDS analyses. Vibrational spectroscopy (ATR, Raman) proved that the proportion of Pb representing a function of network former decreases with time. The shift to higher wavelengths indicates a change in Q motifs in the glass structure of the glaze frits or a glass network transition from a Si-O-Pb-O-Si towards a Si-O-Si glass network.*

### INTRODUCTION

Glazes, together with engobes and enamels, belong to the group of all-over surface coatings of ceramic products, which are applied to the shard and subsequently fixed by firing in furnace. During this process, the glaze melts and final properties as adhesion to the substrate, stability of the coefficients of thermal expansion of the glaze and the substrate, transparency or opacity, surface texture and chemical resistance are obtained. These properties are controlled primarily by the composition of the glazes and also by other input parameters or technological processes. For example, the quality of the glaze surface depends significantly on the particle size distribution of the raw glaze, which mainly affects the smoothness, gloss and cleanability of the surface of the final product. The presence of bubbles and crystalline phases also contributes to the smoothness of the surface and therefore also to the mechanical properties of the glazes. If the bubbles are too close to the surface, they can change from closed to open by creating various micro-holes (dimples, pinholes, etc.). These defects have a very negative effect on the corrosion resistance of the glaze [1-5].

Pollutants to which glazed ceramics are exposed either primarily during their use or secondarily during storage or deposit are of variable composition and can lead to serious damage or destruction. During the use of a ceramic glazed product, its surface is exposed to various influences, such as chemical agents, abrasive wear, external environmental conditions, etc. The quality and durability of the product is primarily determined by the characteristics of the glaze [6]. A visual indication of the chemical effect of the surrounding environment is e.g. the loss of gloss and the formation of a corrosion layer or micro-defects which can lead to the deterioration of the glazed surface. Corrosion resistance and its stability have thus become an essential parameter of the use of glazes and can be influenced by many factors, which can be summarized into three groups [7]: environmental factors (temperature, relative humidity, exposure time, presence of pollutants or microorganisms, etc.), physical conditions of degradation (dynamic or static, S/V ratio, etc.), and the material properties of the object that is exposed to degradation (composition, homogeneity, thermal history, surface morphology etc.).

The complex mechanism of corrosion of glassy phase of glazes can be expressed as the study of the

main reactions of glassy phase of vitreous coating in aqueous media with different pH. Depending on the amount of water condensed on the surface, the process of corrosion can be characterised as corrosion by air (the effect of water vapour and other gaseous pollutants) or corrosion by solutions. Changes in ambient temperature and relative humidity can lead to the precipitation of a microporous layer and affect further interaction with the corrosion medium or even peeling of the corrosion products [8].

The dissolution process in a liquid medium has been extensively studied in various types of glass, analysing several parameters such as reaction medium, chemical composition of glass, temperature, etc. [9-18]. Although ceramic glazes are very similar to glass, studying the dissolution process and overall corrosion is more complicated due to high number of components in glaze raw materials and the variable microstructure of glazes. However, the study of glass can be a guide for a comprehensive description and prediction of glaze degradation. The relative impact of individual processes is influenced mainly by the chemical composition of the glaze material and the corrosion conditions.

The main objective of this work is to study the corrosion behaviour of two types of lead silicate glazes, which were selected based on chemical and mineralogical characterization of archaeological glazed ceramic fragments from the deposits and waste pits of Prague Palaces and surrounding areas. In addition, the work includes the characterization of the surfaces of the corroded archaeological glazes by optical microscopy and infrared reflectance spectroscopy. The results were used to propose corrosion mechanisms in the glazes.

## EXPERIMENTAL

The first part of the experimental part was focused on surface characterisation of several archaeological fragments of glazed ceramics. Ceramic samples and their corrosion products were characterised in terms of chemical and mineralogical composition and based on these analyses model lead silicate fritted glazes for leaching corrosion tests were prepared. The corrosion tests in aqueous environments were accelerated by high concentration of leaching medium, temperature, pressure and humidity.

## Materials preparation

### Archaeological finds

The analysed archaeological finds were selected from a wide variety of available glazed ceramic shards which were found during several archaeological excavations of the Prague Castle complex and surrounding Prague Palaces in the Hradčany district. The representative fragments of stove tiles, tableware, kitchenware and technical ceramics were chosen from the extensive set of Early Modern Age archaeological ceramic finds.

### Model glazes

Two types of fritted glazes of lead silicate system with variable molar ratio of PbO/SiO<sub>2</sub> were prepared from micromilled silica sand (d<sub>50</sub> = 16 µm) and high lead glass frit. The glaze batches were melted in platinum crucibles at 1250 °C (frit 1) and 1350 °C (frit 2) in an electric furnace.

The prepared glaze samples were grinded using a planetary mill (Pulverisette 7, Fritsch, Germany). The finely grounded powders were homogenised and pressed by a hydraulic press to compact samples, which were dried at temperature 105 °C to constant weight. Dried blocks were fired at 900 °C with a heating rate of 5 °C·min<sup>-1</sup> and a dwell time of 10 min at the maximum firing temperature. The fired blocks were ground into fractions of 500 – 250 µm and cleaned ultrasonically in water.

The chemical composition of both glazes (Table 1) corresponding to the chemical compositions of most tested archaeological glazes was determined by X-Ray fluorescence analysis (XRF).

The mineralogical composition of the prepared frits was determined using X-Ray diffraction analysis (XRD). No crystalline phase was identified in glaze frit 1. Quartz was identified as a minor component in glaze frit 2.

### Corrosion test procedure

The corrosion tests in aqueous leaching media were performed in Teflon-lined autoclaves, which were cleaned in 3 % HF solution before the experiment. Acetic and nitric acid solutions were chosen as simple corrosion systems. The static leaching test was selected to simulate conditions of long-time deposition in soil. The leaching

Table 1. Chemical composition prepared lead silicate glazes determined by XRF (wt. %) and converted to mol. % (mol. %).

	SiO <sub>2</sub>	Al <sub>2</sub> O <sub>3</sub>	Fe <sub>2</sub> O <sub>3</sub>	TiO <sub>2</sub>	CaO	ZnO	K <sub>2</sub> O	Na <sub>2</sub> O	PbO	ZrO <sub>2</sub>
Content [wt. %]										
Frit 1	30	7	0.03	0.02	0.3	0.1	0.04	0.0	63	0.05
Frit 2	39	6	0.04	0.02	0.2	0.1	0.04	0.1	54	0.04
Content [mol. %]										
Frit 1	58	8	0.02	0.03	0.6	0.1	0.05	0.0	33	0.05
Frit 2	68	6	0.03	0.03	0.4	0.1	0.04	0.2	25	0.03

media were not renewed or stirred during the experiment. The prepared model glaze frits were exposed for 1, 5 and 10 hours and 1, 2, 3, 7, 14, 30, 60 and 90 days in a pH = 2 solutions at an elevated temperature of 90 °C. The pH value was chosen according to the analyses of the content of the waste wells and literature data [16]. The concentration of corrosive media and conditions of elevated temperature and pressure were chosen based on previous pilot studies [19-21] and comparison with other studies [9, 12, 16, 22-24]. A simple corrosive system of nitric acid solution simulates nitrates in the soil that surrounds the archaeological finds and the aqueous solution of acetic acid represents corrosion in complex organic acids and could be selected as a substitute for humic acids. The surface area per unit of solution volume  $S/V$  was set to match approximately  $2 \text{ cm}^{-1}$ . The surface area was calculated from approximations that the frit particles have a spherical shape with the same diameter  $375 \mu\text{m}$  (the arithmetic mean of the fraction), each particle is in contact with the solution and they form a regular lattice or grid.

#### Analyses of solutions

The solutions after the corrosion tests were cooled to laboratory temperature. The concentrations of Pb and Si in the solution were determined by atomic absorption spectroscopy (AAS) using a 280FS AA spectrometer with a flame atomiser (Agilent Technologies, USA). The detection of Pb was performed with an acetylene-air flame with wavenumber 217 nm, and an acetylene-nitrous oxide flame with wavenumber 261.6 nm was used for the Si analyses. The measurement of pH in the solutions was done before and after the corrosion tests using universal indicator papers and a potentiometric pH meter (inoLab pH Level 1, WTW, UK) with a combination electrode SenTix 81 for accurate measurements.

The results from AAS were converted to normalised mass loss  $NL_i$  to ensure the comparability of the results obtained, which is defined as [9, 22, 25, 26]:

$$NL_i = \frac{C_i V}{x_i S} \quad (1)$$

where  $C_i$  is the concentration of the element  $i$  in solution ( $\text{mg}\cdot\text{l}^{-1}$ ),  $V$  is the volume of solution ( $\text{m}^3$ ),  $x_i$  is the mass fraction of the element in the original composition of the glaze and  $S$  is the reactive surface area considered as geometric surface area in  $\text{m}^2$ .

The data from the corrosion tests were fitted by a Solver add-in program of MS Excel using the nonlinear generalized reduced gradient (GRG) algorithm method. This fitting method was used for the calculation of dissolution of both elements (Pb and Si) due to the approximation that Pb participates in the formation of the glaze structure as a network former, not only as a modifying ion [23, 27-30].

#### Analyses of solid samples of glazes

The initial analyses of degraded surfaces and corrosion products of several archaeological finds were performed using a combination of XRF, XRD, ATR-FTIR and optical microscopy methods.

Solid samples of prepared glaze grits of defined fractions exposed to leaching solutions were observed using stereomicroscopy, polarised light microscopy and scanning electron microscopy with energy-dispersive X-ray spectroscopy before and after exposition to corrosion tests. Optical and electron microscopy were applied for evaluating the homogeneity of the prepared model frits and for the study of the morphology and optical changes of samples before and after exposition to degradation processes. A stereomicroscope Olympus SZX 9 (Olympus, Germany) with a Canon 1100D camera and a polarised light microscope Olympus BX60 (Olympus, Germany) with a Canon 1100D camera were used. The images were processed with Quick Photo Industrial 4.0 software. The scanning electron microscope Tescan VEGA 3 LMU (Tescan Orsay, Czech Republic) with EDS analyser Oxford Instruments INCA 350 were applied for complementary point measurements of chemical composition.

The change in chemical composition of the model samples of glaze frits after leaching were analysed by X-Ray fluorescence (XRF) using a fully-automatic WD-XRF Performix spectrometer with Rh anode, X-ray tube and a scintillation detector. All samples were analysed in the form of fine powders, and the results of semi-quantitative and qualitative analysis are presented in oxide form.

The mineralogical compositions of crystalline corrosion phases on the surface of glazes of model samples subjected to long-term degradation tests and of the fragments of the glazed archaeological ceramics was studied using a PANalytical X'Pert<sup>3</sup> Powder diffractometer (PANalytical, The Netherlands). The mineralogical composition of archaeological glazes was studied on the surfaces of flat ceramic fragments to identify the crystalline phases in the glazes and in the degraded surface layer including corrosion crusts. The data were measured at room temperature with Bragg-Brentano parafocusing geometry using a  $\text{CuK}\alpha$  radiation in the range  $4 - 80^\circ 2\theta$ . The data were evaluated using HighScore Plus 4.0 software package and a reference samples database PDF4<sup>+</sup>.

The analysis of changes in molecular bonding occurring on and near the surface of glaze frits exposed to leaching was carried out using attenuated total reflectance in Fourier transformed infrared spectroscopy method (FTIR-ATR) and Raman spectroscopy. Both experimental analyses were performed at laboratory temperature, for the infrared analysis the Nicolet™ iS50 FTIR Spectrometer (Thermo Fisher Scientific, USA) equipped with a monolithic diamond ATR crystal and

DLaTGS detector was used. The spectra were obtained in absorption mode with 64 scans and resolution  $4\text{ cm}^{-1}$ . The Raman experiments were done using a 532 nm laser and a BWTek i-Raman® Pro spectrometer equipped with a CCD detector (Metrohm, USA). The spectra were acquired in 100 seconds with 1000 collections per second, resolution  $3.5\text{ cm}^{-1}$  and laser power of 50 mW. The infrared and Raman spectra were processed using Omnic 9 software.

## RESULTS AND DISCUSSION

### Archaeological glazed finds

The chemical composition of selected glazes of archaeological finds ranges from 17 – 31 mol. % PbO and 47 – 66 mol. % SiO<sub>2</sub>. The study of the surface of the archaeological glazes include the identification of mineralogical composition of glazes and corrosion products on their surfaces by XRD, photo documentation of degraded surfaces by microscopic images and confirmation of composition of corrosion products removed from the surface of the glazes from FTIR-ATR spectra. Table 2 presents the summary of relevant obtained data.

Most of the examined archaeological fragments were degraded, and several types of disturbed areas were visible to the naked eye. The types of defects were identified by optical microscopy. The chemical composition of corrosion products show CaO, SiO<sub>2</sub> and P<sub>2</sub>O<sub>5</sub> as main components with a lower proportion of MgO, PbO and Fe<sub>2</sub>O<sub>3</sub> in some cases. Crystalline phases identified in mostly amorphous glazes include quartz, phosphates and acetates. Phosphates were identified as dominant corrosion products by both XRD and infrared spectroscopy. Other types of corrosion phases were not clearly identified on the glazed surface or in the studied corrosion products due to their hygroscopicity or fragility. However, XRF analysis of examined glazes and corrosion products show an elevated content of phosphorus (11 – 21 wt. % P<sub>2</sub>O<sub>5</sub>), chlorine (3 wt. %

or sulphur (5 – 7 wt. % SO<sub>3</sub>). Sulphates, chlorides and nitrates were determined in the soil samples from waste pits in concentration up to  $5563\text{ mg}\cdot\text{kg}^{-1}$ . The pH value of most soil samples was slightly acidic.

### Corrosion tests in acid environment

The concentration of Pb and Si analysed in solution by AAS and converted to normalized amounts of the element  $NL_i$  [ $\text{g}\cdot\text{m}^{-2}$ ] transferred into solution is shown in Figure 1. An increase in pH was observed during the leaching process, when the first change in the pH value was clearly detected already after 24 hours.

The time dependence of the leaching of lead and silica ions corresponds to standard static leaching tests of glasses. Therefore the obtained data were fitted by a function [26] using the Microsoft Excel add-in program Solver, using normalised mass loss  $NL_i$  as objective, with the generalized reduced gradient (GRG) nonlinear algorithm method.

The results show that the measured data, with few exceptions, fit well with the course of corrosion of most glasses, where at the beginning of corrosion there is an exponential increase in the dissolved amounts of both ions, and then the corrosion rate slows down and becomes constant over time. Both glazes show deviations from the linear trend. A resumption is observed after about 60 days, this resumption in the corrosion process is probably caused by a combination of several factors, mainly the composition of the glaze frits, the high temperature of the corrosion test and the high S/V ratio [31]. This renewal of corrosion process correlates with the precipitation of secondary phases, which were confirmed by microscopic observations of both types of glaze compositions in both media (Figures 1 and 3).

The release of studied elements from glaze frits change the pH of non-buffered corrosion media as expected. This modification in pH values, although not very significant in both types of media, in conjunction with other factors may contribute to the resumption of the corrosion process. Si/Pb mass ratios in both frits before and after corrosion tests were calculated from XRF data of glaze frits (Table 3). The Si/Pb mass ratios

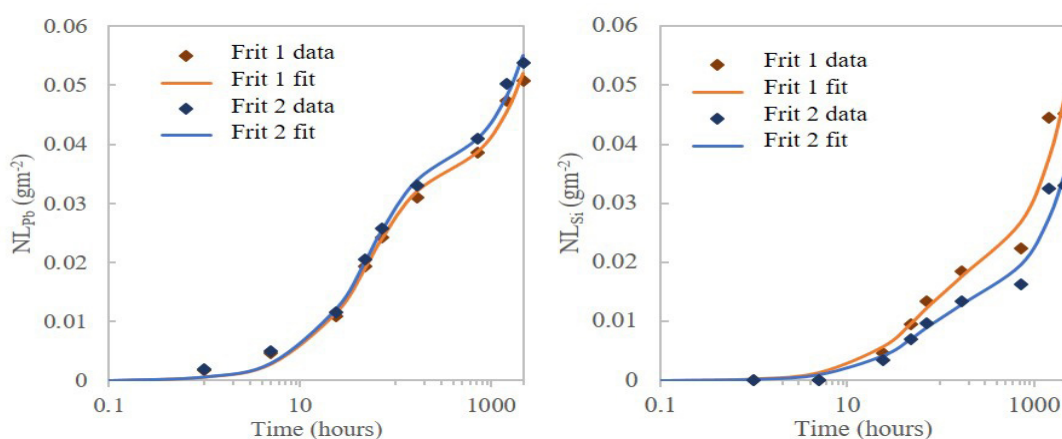


Figure 1. Normalised amount of Pb and Si transferred to nitric acid solution

Table 2: Main results obtained by analyses of archaeological samples.







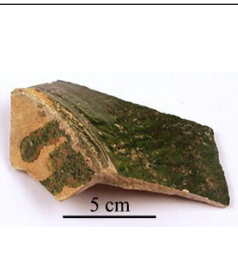
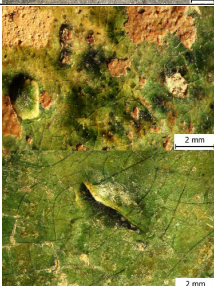

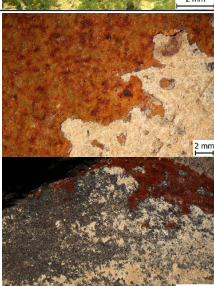
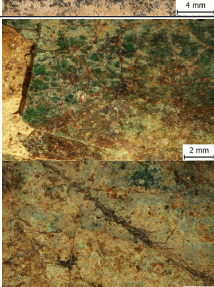

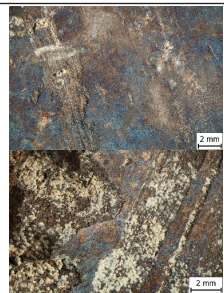

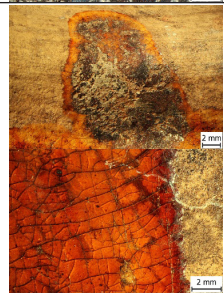

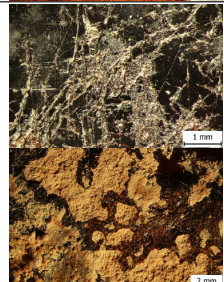
Photo documentation	Microscopic image	Identified defects	Main oxides in corrosion	Identified mineralogical composition of corrosion
		specking, pinholes, crazing	Corrosion not present	
		large deposit of brittle crust	CaO 62 wt. % SiO <sub>2</sub> 26 wt. % MgO 7 wt. %	Calcite CaCO <sub>3</sub> Quartz SiO <sub>2</sub>
		unglazed, compact corrosion crust	CaO 49 wt. % P <sub>2</sub> O <sub>5</sub> 44 wt. %	Hydroxyapatite Ca <sub>5</sub> (PO <sub>4</sub> ) <sub>3</sub> (OH)
		peeling, crazing, blistering	CaO 36 wt. % P <sub>2</sub> O <sub>5</sub> 35 wt. % PbO 11 wt. %	Calcium Phosphate Ca <sub>3</sub> (PO <sub>4</sub> ) <sub>2</sub>
		crazing, specking	P <sub>2</sub> O <sub>5</sub> 48 wt. % CaO 43 wt. %	Calcium Phosphate Ca <sub>3</sub> (PO <sub>4</sub> ) <sub>2</sub>
		crazing, peeling, droppers	Corrosion could not be sampled	

Photo documentation	Microscopic image	Identified defects	Main oxides in corrosion	Identified mineralogical composition of corrosion
		unglazed, salt efflorescence, iridescence	P <sub>2</sub> O <sub>5</sub> 45 wt. % Fe <sub>2</sub> O <sub>3</sub> 17 wt. % SiO <sub>2</sub> 15 wt. % MgO 12 wt. %	Magnesium Iron Phosphate Hydrate Mg <sub>7</sub> Fe <sub>3</sub> (PO <sub>4</sub> ) <sub>3</sub> (H <sub>2</sub> O) <sub>8</sub>
		crazing, speckling, blisters	Could not be sampled	Calcium Phosphate Ca <sub>3</sub> (PO <sub>4</sub> ) <sub>2</sub>
		crazing, peeling, blisters	CaO 84 wt. % SiO <sub>2</sub> 6 wt. % PbO 5 wt. %	Calcite CaCO <sub>3</sub>

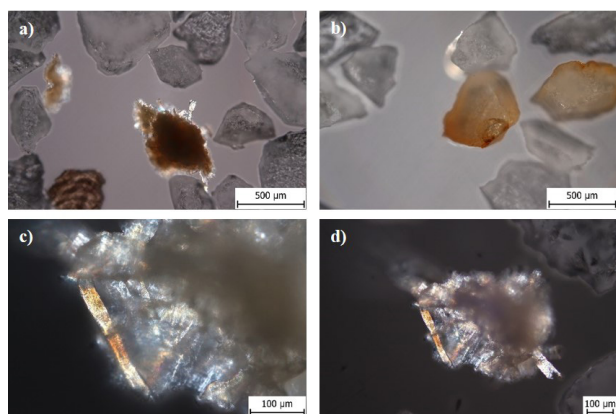


Figure 2. Microscopic images of glaze frits after corrosion test in nitric acid solution: a-b) colourless frit grains and crystalline particles on the surface of glaze frit 1 and c-d) crystalline particles in the form of interlocking rods completely envelop the particle of glaze frit 2.

in the solution were determined by atomic absorption spectroscopy (AAS).

Clusters of elongated particles at the edges of the frit particles were identified by optical microscopy to be secondary precipitation products. In both solutions a discoloration of the frit particles was observed: the frit 1 fragments have yellowish reflections (see Figure 2), while the frit 2 fragments have significant discoloration into bluish reflections (see Figure 4). The changes of colour in time could indicate a modification of the optical properties of the studied frits with the alteration progression. The precipitation products of secondary phases were examined via XRD and SEM-EDS analyses. Crystalline corrosion products in the form of lead nitrate were determined by XRD analysis only in a sample of glaze frit 1 with a higher proportion of PbO after the longest exposure time of the corrosive nitric acid solution. The SEM micrographs showed the degradation

Table 3. Si/Pb ratio in both frits before and after corrosion and in solution (wt. %).

	<i>Si/Pb ratio in frits</i>			<i>Si/Pb ratio in solution</i>	
	<i>before corrosion test</i>	<i>after test in nitric acid solution</i>	<i>after test in acetic acid solution</i>	<i>after test in nitric acid solution</i>	<i>after test in acetic acid solution</i>
<i>Frit 1</i>	0.441	0.652	0.719	0.455	0.153
<i>Frit 2</i>	0.642	0.487	0.747	0.290	0.189

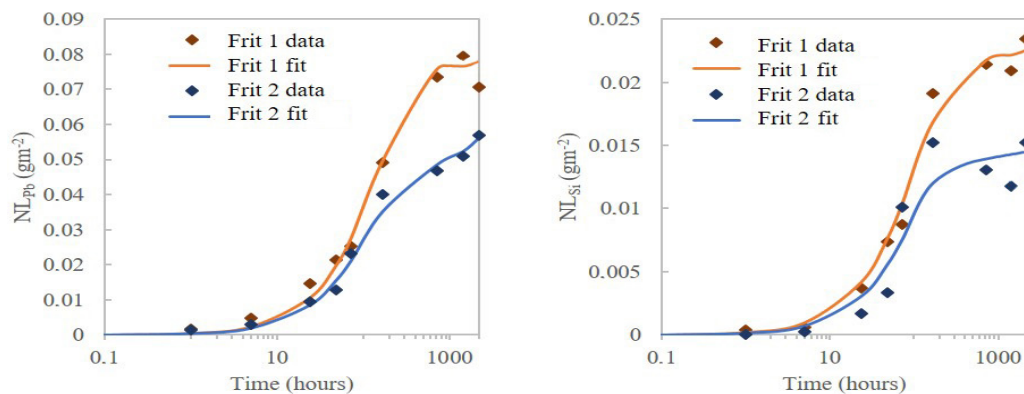


Figure 3. Profiles of normalised mass losses of Pb and Si in time for corrosion by acetic acid solutions for lead silicate frits 1 and 2.

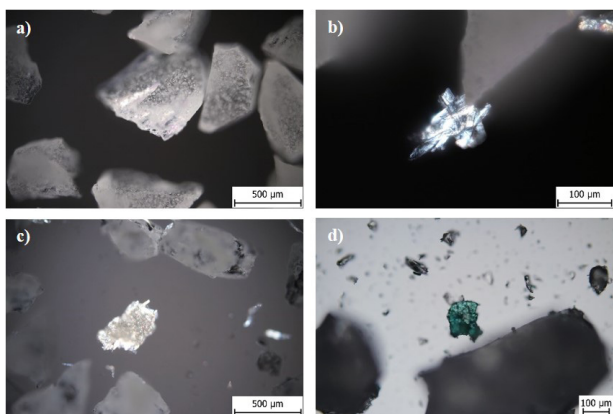


Figure 4. Microscopic images of glaze frits after corrosion test in acetic acid solution: a-b) noticeable disruption of frit 1 particles and growth of the secondary phase at the particles edges and c-d) discoloured particles of frit 2 and the particles completely covered with secondary phases

of particles and signs of corrosion in both lead-silicate glaze frits. At the edges and corners of most frit particles, the growth of corrosion products was confirmed.

The crystalline phase identified via XRD analysis were observed as a cluster of interconnected flat rod-shaped needles (Figure 5a-c), the main component of these particles analysed by EDS was Pb, accompanied by a small proportion of Si and Al. Another indication

of preferable local pitting corrosion was evident in both types of glaze frits in the form of dehydrating cracks as the first phase of corrosion. Dehydration cracks, which result in flaking of hydrated surfaces, were observed in micrographs of glaze frits of both compositions (Figure 5f and h). Most often, these defects occur at the edges of individual particles. The significant difference between alterations of surfaces by nitric acid or acetic acid media are that in  $\text{HNO}_3$  the flaking of secondary phases is more obvious and frequent. However, the effects of acetic media are more visible in the formation of dehydration cracks and depletion of the disrupted areas (mostly edges of particles). Furthermore, the formation of local electrolytes can be detected at the edges of some particles where there is a local increase in pH, and a subsequent change in the corrosion mechanism from interdiffusion of ions to the dissolution of the glass matrix of glaze particles occurs (see Figure 5d, e and g). The preferential precipitation of the corrosion products at new surfaces (in the corrosion cracks) was confirmed in both corrosive media (Figure 5h).

Dimples with a higher proportion of Si analysed via EDS were observed on the flat surfaces of both frits (Figure 5i), the formation of pinholes is assumed to depend on stresses or minor compositional differences. In these regions, most of the lead cations could be bonded as a modifier.

The results of measurements by vibrational

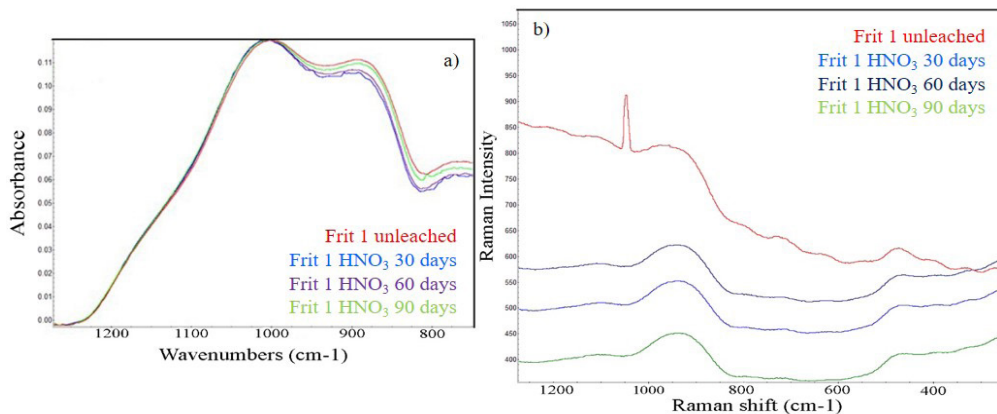


Figure 6. Vibration spectra of unaltered and corroded frits: a) ATR spectra of frit 1 exposed to nitric acid solutions and b) detail of Raman spectra of frit 1 corroded in  $\text{HNO}_3$  in time dependence.

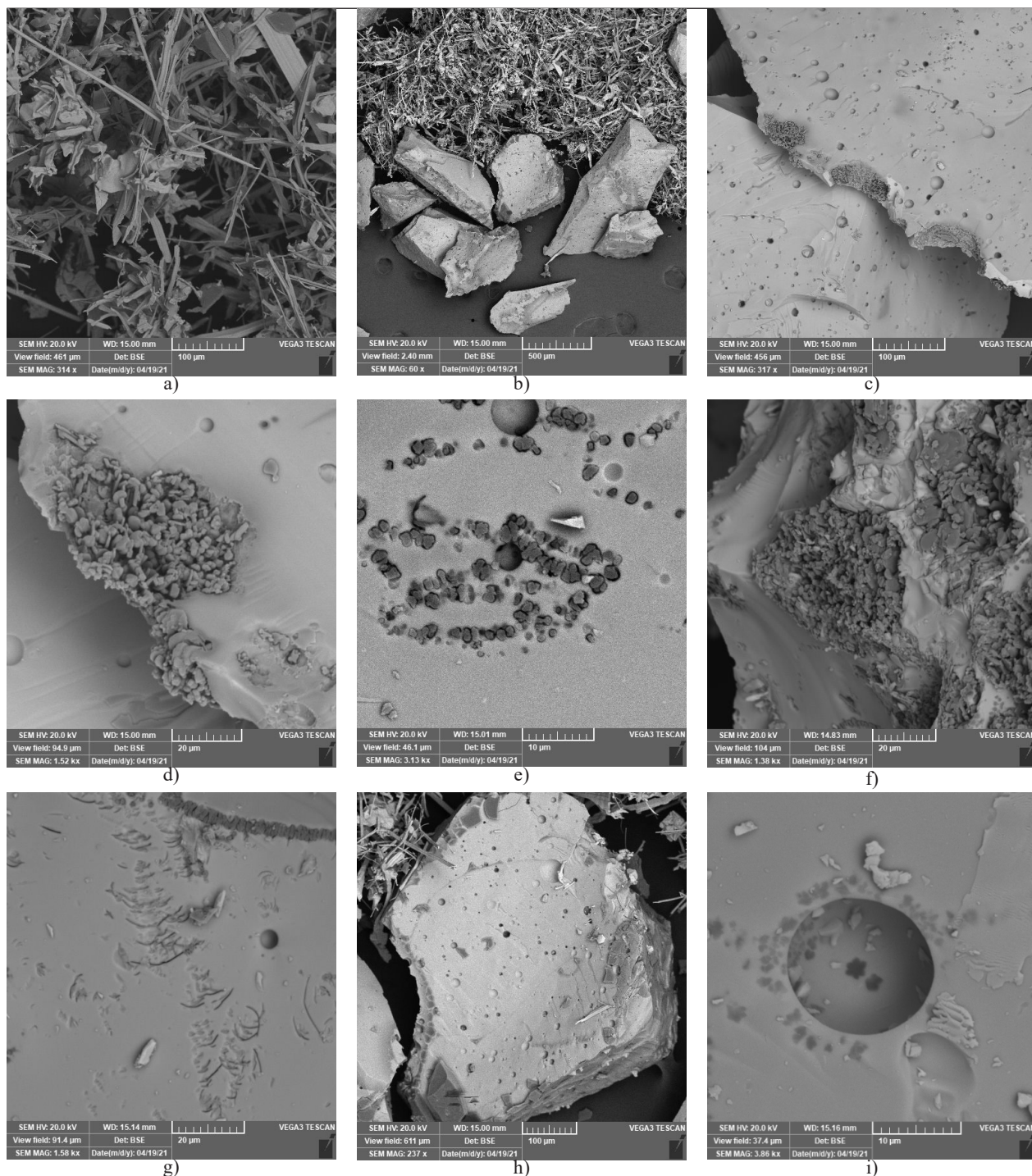


Figure 5. SEM micrographs of lead-silicate glaze frits 1 and 2 after alteration: a-b) large amount clusters of secondary phase with high proportion of Pb, c) surface of altered particle of frit 1 with dehydration cracks and detached flake particles, d-e) local snaps on the edge of glaze frit 1 particle in acetic media, f) surface of frit 2 with cracks and signs of localised alterations, g) edges of frit 2 severely corroded by acetic acid solution, h) corrosion pinholes filled with secondary products and i) surface defects around bubble in the form of dimples.

spectroscopy (ATR, Raman) confirmed that the proportion of  $Pb^{2+}$  involved in the glass structure of glaze matrix representing a function of network former decreases with time, and the shift to higher wavelengths indicates a change in Q motifs in the glass structure of both glaze frits. The precipitation of secondary phases during alteration could be also partially observed in

Raman spectra of the frit 1, where the sharp peak at  $1100\text{ cm}^{-1}$  can be attributed to the  $NO_3^-$  group. The nitrate group was confirmed by a small band at  $720\text{ cm}^{-1}$  in ATR spectra of both frits, but no other nitrate peaks were detected by vibration spectroscopy and thus their presence is not conclusive. In ATR spectra comparison of frits 1 and 2, a slight shift towards higher wavelength



was determined at band  $1000\text{ cm}^{-1}$ , which corresponds to  $(\text{SiO}_4)^{4-}$  tetrahedral stretching vibrations. The shoulder band at  $900\text{ cm}^{-1}$  is related to the presence of  $\text{Pb}^{2+}$  as a network former, and the decreasing trend and shift to higher wavelengths was observed in all studied spectra with increasing time of the corrosion leaching tests. The region  $400 - 600\text{ cm}^{-1}$  (main peaks  $400, 490$  and  $600\text{ cm}^{-1}$ ) in Raman spectra is characteristic for vitreous silica and the vibration of bridging oxygen in silica tetrahedra. With increasing leaching time, an obvious change in the intensity of the region bands was determined, so it could be concluded that the glass network in the glaze matrix changes from a Si-O-Pb-O-Si towards a Si-O-Si glass network. The change of intensity and shift to higher wavenumbers of the band  $950\text{ cm}^{-1}$  is attributable to modification of the  $\text{Q}_{\text{Si}^n}$  structural units, which confirms ATR spectra when the amount of Pb involved in matrix formation decreases.

## CONCLUSIONS

The results presented indicate that the corrosion tests in acid solutions could simulate the degradation process of historical glazes, as similar corrosion products were detected by XRD. The comparison of AAS, XRF, SEM and ATR analysis show that the overall Si to Pb ratio in the glaze matrix mainly affected the alteration in acetic acid solutions where in frit with higher ratio more Pb and less Si was transferred to solution. Raman and ATR spectra indicate differences in peak shape and wavenumber shifts in spectra caused by the corrosive action of the solutions. The blue shifts in Raman spectra is attributed to a change in the  $\text{Q}_{\text{Si}^n}$  structural units. The process of corrosion of lead silicate glazes follows the alteration kinetics generally considered for most glasses.

## Acknowledgements

*This work was financially supported by the project of the Ministry of Culture of the Czech Republic: Technology of Treatment and Identification of Degradation Processes of Ceramic Finds from Hradčany Palaces—Methods of Restoration and Conservation of Porous and Dense Ceramics and Porcelain (NAKI II DG18P02OVV028).*

## REFERENCES

- Li J., Liang J., Wang F., Wang L. (2014): The role of firing process on bubble formation in a glaze layer of sanitary ware. *Thermochimica Acta*, 588, 75-80. doi: 10.1016/j.tca.2014.03.024
- Abdelaziz T.D., Ezz-Eldin F.M. (2018): Influence of industrial solid waste on the chemical and mechanical properties of traditional glaze-ceramics. *Silicon*, 10(2), 471-482. doi:10.1007/s12633-016-9477-x
- Fröberg L., Kronberg T., Törnblom S., Hupa L. (2007): Chemical durability of glazed surfaces. *Journal of the European Ceramic Society*, 27(2-3), 1811-1816. doi:10.1016/j.jeurceramsoc.2006.04.162
- Kronberg T., Hupa L. (2020): The impact of wollastonite and dolomite on chemical durability of matte fast-fired raw glazes. *Journal of the European Ceramic Society*, 40(8), 3327-3337. doi: 10.1016/j.jeurceramsoc.2020.03.033
- Hupa L., Bergman R., Fröberg L., Vane-Tempest S., Hupa M., Kroberg T., Pesonen-Leinonen E., Sjöberg A.M. (2005): Chemical resistance and cleanability of glazed surfaces. *Surface Science*, 584(1), 113-118. doi:10.1016/j.susc.2004.11.048
- Kopar T., Ducman V. (2007): Low-vacuum SEM analyses of ceramic tiles with emphasis on glaze defects characterisation. *Materials Characterization*, 58(11-12), 1133-1137. doi:10.1016/j.matchar.2007.04.022
- Clark D.E., Zaitos B.K. (1992). *Corrosion of glass, ceramics and ceramic superconductors: principles, testing, characterization and applications*. 1st ed. Noyes Publications.
- Römich H. (1999). Historic glass and its interaction with the environment, in: Tennent N.H. *The conservation of glass and ceramics: research, practise and training*. James & James. pp 5-14.
- Cailleteau C., Weigel C., Ledieu A., Barboux P., Devreux F., (2008): On the effect of glass composition in the dissolution of glasses by water. *Journal of Non-Crystalline Solids*, 354(2-9), 117-123. doi:10.1016/j.jnoncrysol.2007.07.063
- Majerus O., Lehuédé P., Biron I., Alloteau F., Narayanasamy S., Caurant D. (2020): Glass alteration in atmospheric conditions: crossing perspectives from cultural heritage, glass industry, and nuclear waste management. *Npj Materials Degradation*, 4(1). doi:10.1038/s41529-020-00130-9
- Abrajano T.A., Bates J.K., Byers C.D. (1986): Aqueous corrosion of natural and nuclear waste glasses I. Comparative rates of hydration in liquid and vapor environments at elevated temperatures. *Journal of Non-Crystalline Solids*, 84(1-3), 251-257. doi:10.1016/0022-3093(86)90783-0
- Rahimi R.A., Sadrnezhad S.K., Raisali G. (2009): Hydrolysis kinetics of lead silicate glass in acid solution. *Journal of Nuclear Materials*, 389(3), 427-431. doi:10.1016/j.jnucmat.2009.02.028
- Robinet L., Hall C., Eremin K., Fearn S., Tate J. (2009): Alteration of soda silicate glasses by organic pollutants in museums: Mechanisms and kinetics. *Journal of Non-Crystalline Solids*, 355(28-30), 1479-1488. doi:10.1016/j.jnoncrysol.2009.05.011
- Gibson L.T., Watt C.M. (2010): Acetic and formic acids emitted from wood samples and their effect on selected materials in museum environments. *Corrosion Science*, 52(1), 172-178. doi:10.1016/j.corsci.2009.08.054
- Van Elteren J.T., Grile M., Beeston M.P., Reig M.S., Grgić I. (2013): An integrated experimental-modeling approach to study the acid leaching behavior of lead from sub-micrometer lead silicate glass particles. *Journal of Hazardous Materials*, 262, 240-249. doi:10.1016/j.jhazmat.2013.08.052
- Bonnet C., Bouquillon A., Turrell S., Deram V., Mille B., Salomon J., Thomassin J.H., Fiaud C. (2003): Alteration of lead silicate glasses due to leaching in heated acid solutions. *Journal of Non-Crystalline Solids*, 323(1-3), 214-220. doi:10.1016/S0022-3093(03)00279-5
- Rahimi R.A., Sadrnezhad S.K., Raisali G. (2009): Chemical

- durability of lead silicate glass in HNO<sub>3</sub>, HCl and H<sub>2</sub>SO<sub>4</sub> aqueous acid solutions. *Journal of Non-Crystalline Solids*, 355(3), 169-174. doi:10.1016/j.jnoncrysol.2008.11.001
18. Alloteau F., Lehuédé P., Majérus O., Biron I., Dervanian A., Charpentier T., Caurant D. (2017): New insight into atmospheric alteration of alkali-lime silicate glasses. *Corrosion Science*, 122, 12-25. doi:10.1016/j.corsci.2017.03.025
  19. Kavanová M. (2018). *Degradation of glazes - dissertation*. UCT Prague. Supervisor A. Kloužková.
  20. Kolářová M., Kloužková A., Kloužek J., Schwarz J. (2020): Thermal behaviour of glazed ceramic bodies. *Journal of Thermal Analysis and Calorimetry*, 142(1), 217-229. doi:10.1007/s10973-020-09484-3
  21. Kloužková A., Kohoutková M., Kolářová M., Blažková G., Šefců R., Dvořáková P., Bajoux Kmoníčková M. (2020): Multi-methodical study of Early Modern Age archaeological glazed ceramics from Prague. *Heritage Science*, 8(1). doi:10.1186/s40494-020-00423-x
  22. Sessegolo, L., Verney-Carran A., Ausset P., Nowak S., Triquet S., Saheb M., Chabas A. (2020): Alteration rate of medieval potash-lime silicate glass as a function of pH and temperature: A low pH-dependent dissolution: A low pH-dependent dissolution. *Chemical Geology*, 550, 119704. doi: 10.1016/j.chemgeo.2020.119704
  23. Wood S., a Blachere J. R. (1978): Corrosion of lead glasses in acid media: I, Leaching kinetics. *Journal of the American Ceramic Society*, 61(7-8), 287-292. doi:10.1111/j.1151-2916.1978.tb09310.x
  24. Bertoncello R., Milanese L., Bouquillon A., Dran J.C., Mille B., Salomon J. (2004): Leaching of lead silicate glasses in acid environment: compositional and structural changes. *Applied Physics A*, 79(2), 193-198. doi:10.1007/s00339-004-2651-9
  25. Ebert W. (1995). *The effects of the glass surface area/ solution volume ratio on glass corrosion: A critical review*. Argonne National Laboratory Report.
  26. Helebrant A., Tosnerova B. (1989): Mathematical model used to compare glass durability tests under different flow conditions. *Glass Technology*, 30, 220-223.
  27. Doménech-Carbó A., Doménech-Carbó M. T., Gimeno-Adelantado J.V., Bosch-Reig F. (2000): Voltammetric identification of lead(II) and (IV) in mediaeval glazes in abrasion-modified carbon paste and polymer film electrodes. Application to the study of alterations in archaeological ceramic. *Electroanalysis*, 12(2), 120-127. doi: 10.1002/(SICI)1521-4109(200002)12:2<120::AID-ELAN120>3.0.CO;2-E.
  28. Angeli F., Jollivet P., Charpentier T., Fournier M., Gin S. (2016): Structure and chemical durability of lead crystal glass. *Environmental Science & Technology*, 50(21), 11549-11558. doi: 10.1021/acs.est.6b02971.
  29. Fayon F., Bessada C., Massiot D., Farnan I., Coutures J.P. (1998): 29Si and 207Pb NMR study of local order in lead silicate glasses. *Journal of Non-Crystalline Solids*, 232-234, 403-408. doi: 10.1016/S0022-3093(98)00470-0.
  30. Wang P.W., Zhang L. (1996): Structural role of lead in lead silicate glasses derived from XPS spectra. *Journal of Non-Crystalline Solids*, 194(1-2), 129-134. doi: 10.1016/0022-3093(95)00471-8.
  31. Gin S., Abdelouas A., Criscenti L.J., Ebert W.L., Ferrand K., Geisler T., Harrison M.T., Inagaki Y., Mitsui S., Mueller K.T., Marra J.C., Pantano C.G., Pierce E.M., Ryan J.V., Schofield J.M., Steefel C.I., Vienna J.D. (2013): An international initiative on long-term behavior of high-level nuclear waste glass. *Materials Today*, 16(6), 243-248. doi:10.1016/j.mattod.2013.06.008